Numerical trajectory calculations for the efficient inversion of transient flow and tracer observations

D. W. Vasco and Stefan Finsterle

Berkeley Laboratory, University of California, Berkeley, California, USA

Received 27 May 2003; revised 26 September 2003; accepted 15 October 2003; published 8 January 2004.

[1] We introduce a trajectory-based method for the inversion of flow and transport observations. The approach operates on the output of a standard numerical simulator and is applicable under very general conditions. Using only head and concentration histories, we efficiently construct the model parameter sensitivities required for solving the inverse problem. A single simulation or forward calculation is required in order to take a step in the inversion. Our formulation, based on asymptotic solutions for flow and transport, partitions the inverse problem into an arrival time and an amplitude-matching problem. Because the model parameter sensitivities are defined along trajectories, both inverse problems scale very well with respect to model size. At the migration experimental site of the Grimsel Rock Laboratory in Switzerland we utilized transient head and tracer arrival times to constrain the hydraulic conductivity between a suite of boreholes. The squared data misfit is reduced by over an order of magnitude in 30 iterations of our inversion algorithm. Each iteration requires two runs of our numerical simulator TOUGH2, one for each experiment, to construct the trajectories and associated model parameter sensitivities. We find a high-conductivity channel curving in a roughly east-west direction, in agreement with two previous studies. Estimates of model parameter resolution indicate that we can image the large-scale conductivity variations within the array of boreholes. *INDEX TERMS:* 1829 Hydrology: Groundwater hydrology; 1832 Hydrology: Groundwater transport; 1894 Hydrology: Instruments and techniques; 3260 Mathematical Geophysics: Inverse theory; *KEYWORDS:* characterization, inverse modeling, inversion, streamline, tracer, transient flow

Citation: Vasco, D. W., and S. Finsterle (2004), Numerical trajectory calculations for the efficient inversion of transient flow and tracer observations, *Water Resour. Res.*, *40*, W01507, doi:10.1029/2003WR002362.

1. Introduction

[2] Over the past several decades there have been significant advances in the capabilities of reservoir simulators. Numerical simulators can account for thermal effects as well as phase changes [*O'Sullivan et al.*, 2001]. Many varieties of coupled simulators have been developed. For example, there are simulators which account for reactive transport and radioactive decay [*Yeh and Tripathi*, 1991; *Xu and Pruess*, 2001; *Xu et al.*, 2001], simulators which model coupled mechanical deformation and fluid flow [*Noorishad and Tsang*, 1996; *Rutqvist et al.*, 2002], and simulators which incorporate biological phenomena [*Rittmann and VanBriesen*, 1996]. Numerical simulators such as these represent a significant investment in time and resources. As such, they are valuable tools for tackling the forward problem of reservoir simulation.

[3] In solving the inverse problem of reservoir characterization we should take full advantage of the sophistication of current numerical simulators. That is, we should develop methods which operate directly on the output of a simulator run. This is already done in techniques that numerically difference simulator runs to calculate the components of the gradient vector for use in an iterative inversion [*Finsterle and Pruess*, 1995]. Also, a stochastic method, such as simulated annealing [*Datta-Gupta et al.*, 1995], operates directly on the output of a numerical simulator in order to update a prior model. Unfortunately, both of these approaches can require significant computation for large three-dimensional models. Alternative approaches, such as the adjoint-state and sensitivity equation methods are more efficient but require significant additional coding to form and solve the adjoint or coefficient equations [*Yeh*, 1986]. There is a need for inverse techniques that require the same level of computation as the solution of the forward problem and yet are easy to implement.

[4] In this paper we introduce a simple yet efficient approach based upon asymptotic solutions to the equations of transient flow and tracer transport. All quantities necessary for taking a step in our inversion algorithm, head and solute concentration histories, are produced by a conventional numerical simulator. In what follows we use the integral finite difference simulator TOUGH2 [*Pruess et al.*, 1999]. We merely post-process the results of a single simulation in order to take a step in our inversion algorithm. The asymptotic solutions are defined along trajectories through the model, much like optical or seismic rays. Thus the solution and model parameter sensitivities only depend on quantities defined along the trajectories. Because of this, the asymptotic approach scales quite well with problem size. The trajectories are the fundamental elements in our

0043-1397/04/2003WR002362

inversion technique, and defining them is an important aspect of our approach. The computer routine for accomplishing this is quite brief, involving of the order of one hundred lines of code. In the asymptotic methodology the data-fitting problem partitions into a kinematic, or travel time matching problem, and a dynamic, or amplitude-matching problem. This provides additional flexibility in the inversion. There is increasing recognition of the utility and advantages of arrival times [*Rubin and Dagan*, 1992; *Harvey and Gorelick*, 1995; *Woodbury and Rubin*, 2000; *Feyen et al.*, 2003]. For example, solute travel times are independent of the amount of tracer injected and less affected by pore-scale dispersivity [*Feyen et al.*, 2003]. Our experience indicates that travel time matching is quite robust and provides a prior model with which to fit the amplitudes [*Vasco and Datta-Gupta*, 1999; *Vasco et al.*, 2000].

[5] The asymptotic approach to inversion was introduced by *Vasco and Datta-Gupta* [1999] for tracer transport and extended to transient head by *Vasco et al.* [2000]. Asymptotic techniques have also proven useful in the inversion of two-phase flow data [*Vasco and Datta-Gupta*, 2001]. In those papers the trajectories required to construct an asymptotic solution were computed using either ray-tracing or streamline simulation. Here we describe how to compute the trajectories directly from the output of a numerical simulator. Note that, for transient flow, the trajectories can differ from streamlines [*Datta-Gupta and King*, 1995; *Crane and Blunt*, 1999]. In this paper we also extend the tracer transport results of *Vasco and Datta-Gupta* [1999] to include general dispersion and hydraulic conductivity tensors. We find that the trajectories for tracer transport depend on the flow field, similar to the situation for streamlines. In fact, the asymptotic methodology provides a mathematical framework for streamline modeling of tracer transport and multiphase flow. Utilzing this framework we can link streamline simulation to ray methods from geometrical optics and geophysics. Our treatment of transient head and tracer transport by no means exhausts the possible applications of asymptotic methods. Asymptotic and related techniques are useful for modeling a wide variety of phenomena such as spiral and toroidal scroll waves, multiple reaction fronts, solitons, fingering [*Grindrod*, 1996] and traveling wave convection [*Knobloch and De Luca*, 1990].

2. Methodology

[6] In this section we describe asymptotic solutions to the equations of transient flow and tracer transport. Asymptotic methods are the basis for fast inversion schemes in optical, medical, and geophysical imaging [*Gordon and Herman*, 1974; *Iyer and Hirahara*, 1993; *Arridge*, 1999]. The methods are applicable to the fully general equations governing the evolution of hydraulic head and solute transport. The asymptotic solutions are specified on trajectories through the model. This property is critical for developing a very efficient inversion scheme. That is, we do not have to specify quantities throughout the model, just on curves through the model. Thus as the model grows in size the amount of information necessary to define an asymptotic solution increases much more slowly. By coupling our asymptotic solutions and a numerical simulator we can develop a general, and easily implemented, methodology for imaging reservoir properties using flow and transport observations.

2.1. Hydraulic Head

[7] In a medium with spatially varying flow properties, the space $\mathbf{x}$ and time t variation in head $h(\mathbf{x}, t)$ is described by the equation

$$S\frac{\partial h}{\partial t} - K\nabla^2 h - \nabla K \cdot \nabla h = 0 \tag{1}$$

where $K(\mathbf{x})$ denotes the hydraulic conductivity and $S(\mathbf{x})$ denotes the storage coefficient [*Bear*, 1972; *de Marsily*, 1986, p. 111]. *Vasco et al.* [2000], building upon earlier work by *Cohen and Lewis* [1967] and *Virieux et al.* [1994], derived an asymptotic solution for equation (1)

$$h(\mathbf{x}, t) = \int_0^t q(t')h_0(\mathbf{x})\frac{\sigma(\mathbf{x})}{2\sqrt{\pi(t-t')^3}}e^{-\sigma^2(\mathbf{x})/4(t-t')}dt' \tag{2}$$

where $q(t')$ is the flow rate, $\sigma(\mathbf{x})$ is a measure of the "propagation time" from the pumping well to the observation point $\mathbf{x}$, and $h_0(\mathbf{x})$ is a solution of a transport equation [*Vasco et al.*, 2000]. In what follows we shall assume that the flow rate $q(t')$ is a step function in which a pump is activated at time zero and maintains a constant value q_0 there after. For more complicated, but known, flow rate variations one can deconvolve the source time variation from the head observations [*Bracewell*, 1978].

[8] An important aspect of the asymptotic solution (2) is that it is defined along one-dimensional trajectories, $\mathbf{X}(r)$, through the medium. For a detailed development and definition of these trajectories, see *Vasco et al.* [2000]. The scalar variable r signifies the distance along the trajectory $\mathbf{X}$. The trajectory $\mathbf{X}(r)$ is determined by the system of differential equations

$$\frac{d\mathbf{X}}{dr} = \mathbf{p} \tag{3a}$$

$$\frac{d\mathbf{p}}{dr} = \nabla\kappa \tag{3b}$$

where $\mathbf{p} = \nabla\sigma$ is a vector perpendicular to the surfaces of constant propagation time and

$$\kappa(\mathbf{r}) = \frac{S(r)}{K(r)}. \tag{4}$$

is the inverse of the diffusivity of the medium. As shown by *Vasco et al.* [2000], in the trajectory-based coordinate system the propagation time from a source point at r_0 to a point r is given by an integral along the trajectory

$$\sigma(r) = \int_{r_0}^{r}\sqrt{\kappa(r')}dr'. \tag{5}$$

We must emphasize that the trajectories $\mathbf{X}(r)$ are defined for fully transient flow and differ from streamlines which are associated with quasi-steady state flow [*Datta-Gupta and King*, 1995; *King and Datta-Gupta*, 1998]. This is clear

from the defining equations (3a) and (3b) which depend on the static flow properties $S(\mathbf{x})$ and $K(\mathbf{x})$ and are independent of time. For a transient problem the streamlines, which depend on the gradient of the head variation, are generally time-dependent.

[9] At this point a short discussion on notation is warranted. Our spatial variables are denoted by $\mathbf{x}$. For example, material properties such as K and S, defined on our simulation grid will be functions of $\mathbf{x}$. Our trajectories are denoted by $\mathbf{X}(r)$ where r signifies the distance along the path. We will often represent quantities define along trajectories, such as σ, as functions of r. However, in our approach, which combines simulation on an underlying grid with trajectory computations, we will switch back and forth between $\mathbf{x}$ and $\mathbf{X}(r)$ coordinates. Thus σ may be defined as a function of either r or $\mathbf{x}$, depending on the coordinate system used. We may compute $\mathbf{x}$ by defining the trajectory from the grid point $\mathbf{x}$ to the injection well and determining where on the trajectory (r) $\mathbf{x}$ lies. Similarly, we may consider K as a function of $\mathbf{x}$ or as a function of r for some appropriate trajectory. In summary then, we are free to switch from grid coordinates to trajectory coordinates and vice versa.

[10] The asymptotic methodology provides a framework for an efficient and robust approach to the inversion of transient pressure and head data. However, deriving the quantities required to construct an asymptotic solution requires solving the ray equations (3a) and (3b), for a given well configuration, boundary conditions, and distribution of flow properties $K(\mathbf{x})$ and $S(\mathbf{x})$. Both in principal and in practice, solving the ray equations is not difficult. However, it does entail two-point ray-tracing which is not common practice in hydrologic modeling. There would be considerable advantage in computing the trajectories $\mathbf{X}(r)$ in equation (3a) directly from the output of a reservoir simulator, without resorting to a two-point ray-tracing code. As shown below, such an approach is entirely feasible.

[11] The basic idea for constructing the trajectory $\mathbf{X}(r)$ is to first compute the variation of head over a grid, using a numerical simulator. That is, at each cell of the simulation grid we compute the temporal variation in head. Then, we make use of the asymptotic form of the solution (2) defined along the trajectory. First, differentiate the expression (2) for $h(\mathbf{x}, t)$ with respect to t

$$\dot{h}(\mathbf{x},t) = q_0 h_0(\mathbf{x}) \frac{\sigma(\mathbf{x})}{2\sqrt{\pi t^3}} e^{-\sigma^2(\mathbf{x})/4t}. \tag{6}$$

Note that we have made use of the step function form of $q(t')$. Differentiating this quantity again with respect to t gives

$$\frac{\partial \dot{h}(\mathbf{x},t)}{\partial t} = q_0 h_0(\mathbf{x}) \frac{\sigma(\mathbf{x})}{2\sqrt{\pi}} e^{-\sigma^2(\mathbf{x})/4t} \left[-\frac{3}{2\sqrt{t^5}} + \frac{\sigma^2(\mathbf{x})}{4\sqrt{t^7}} \right] \tag{7}$$

which has a zero when the quantity in square brackets vanishes, i.e., when

$$t = \frac{\sigma^2(\mathbf{x})}{6}. \tag{8}$$

Thus the phase $\sigma(\mathbf{x})$ is given by

$$\sigma(\mathbf{x}) = \sqrt{6 T_{peak}} \tag{9}$$

where T_{peak} denotes the time at which equation (7) vanishes. This coincides with the peak of the derivative of the transient head curve, as noted by *Vasco et al.* [2000]. Thus the propagation time, $\sigma(\mathbf{x})$, is proportional to the square root of the time at which the head is changing most rapidly. Utilizing the computed head variations in each grid block we can calculate T_{peak} and hence $\sigma(\mathbf{x})$.

[12] Given calculated values for $\sigma(\mathbf{x})$ on the simulation grid we compute $\mathbf{p} = \nabla\sigma(\mathbf{x})$ using finite differences. The trajectories are obtained numerically by stepping down the gradient of $\sigma(\mathbf{x})$, starting at the observation well. The formal procedure we use, a second-order Runge-Kutta technique, is known as Heun's method. Heun's method is quite simple and can be implemented in approximately twenty to thirty lines of computer code. In essence, Heun's method improves upon an Euler iteration by computing the gradient at an intermediate point. That is, after the ith step along the trajectory we take an intermediate step based upon equation (3a)

$$\hat{\mathbf{X}}_i = \mathbf{X}_i - \mathbf{p}(\mathbf{X}_i)\delta r \tag{10}$$

where $\mathbf{p} = \nabla\sigma$. The (i + 1)th step is simply the average of the gradients at $\mathbf{X}_i$ and the intermediate point $\hat{\mathbf{X}}_i$

$$\mathbf{X}_{i+1} = \mathbf{X}_i - \frac{\delta r}{2}\left[\mathbf{p}(\mathbf{X}_i) + \mathbf{p}(\hat{\mathbf{X}}_i)\right]. \tag{11}$$

We should emphasize that, while we are computing the trajectory numerically, based upon equation (3a), we do not solve the two-point boundary value problem itself. Rather, on the basis of equation (9), we let the reservoir simulator determine the distribution of $\sigma(\mathbf{x})$ which satisfies the initial and boundary conditions. If we were to actually determine both $\sigma(r)$ and $\mathbf{X}(r)$ we must solve either the coupled set of differential equations (3) by numerical integration or solve the Eikonal equation using a technique such as the fast marching method [*Sethian*, 1999]. Both procedures require more extensive coding, although there are packages of programs and efficient algorithms to accomplish these tasks [*Press et al.*, 1992; *Sethian*, 1999].

[13] For illustration, consider a two-dimensional example, simulating an interference test. The well configuration and the pattern of hydraulic conductivity are both shown in Figure 1. The pumping well (9) is located at the southernmost edge of an array of boreholes. Overall, there is a central band of high conductivity trending roughly northeast. Using the integral finite difference simulator TOUGH2 [*Pruess et al.*, 1999] we calculate reservoir head variations over a period of 0.17 days. Three snapshots of the drawdown [0.02, 0.04, and 0.12 $\sqrt{\text{days}}$] are shown in Figure 2. Because of the higher conductivity, the distribution of drawdown migrates asymmetrically to the northeast over time. Some idea of the wave-like nature of the transient head can be discerned if one examines the time derivative of head (Figure 3). At times of 0.02, 0.04, and 0.12 $\sqrt{\text{days}}$ we observe the outward propagation of the peak derivative from pumping well 9. The propagation is nonuniform, with faster movement to the northeast and to the west regions of higher conductivity.

[14] The calculated drawdown at each observing well is shown in Figure 4. The slopes of the drawdown curves are also shown in Figure 4. There are notable variations in the

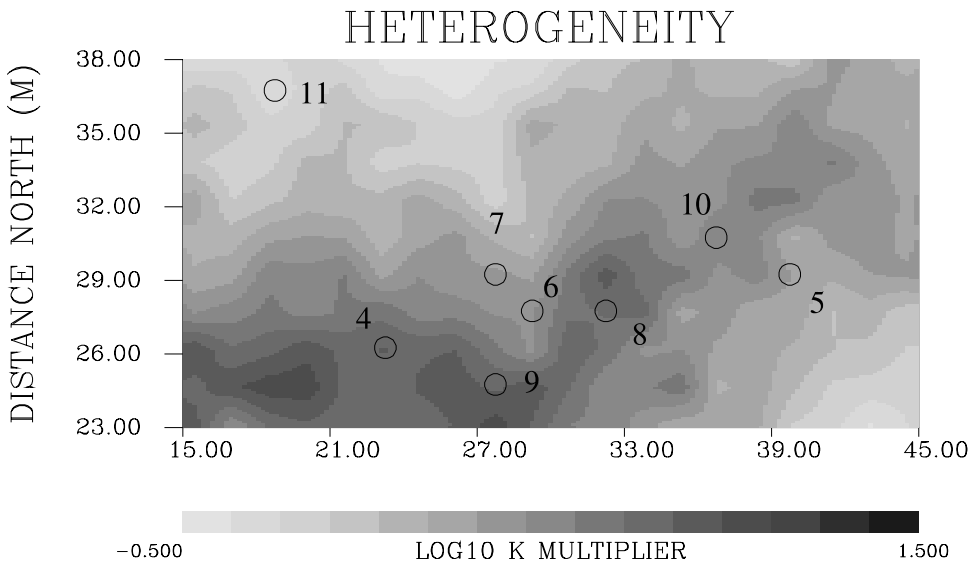

Figure 1. Hydraulic conductivity variation used for numerical trajectory computations. The well locations are denoted by open circles and well numbers. Well 9 serves as the pumping well for these calculations.

arrival times of the peaks. Some of the variation is induced by heterogeneity in the subsurface. For example, the peak slope occurs sooner at borehole 4 than it does at borehole 8, even though these wells are approximately equidistant from the pumping well 9.

[15] Given the history of drawdown in each grid block of the simulator we can compute the peak slope and the associated arrival time. Using equation (9) we then compute the variation of $\sigma(\mathbf{x})$ over the simulation grid (Figure 5). Note that the arrival time is somewhat delayed in the upper northwest of the grid, as expected, considering the lower conductivity found there (Figure 1). Given the distribution of $\sigma(\mathbf{x})$, we compute the trajectories from the observing wells to the pumping well. The trajectories are constructed using Heun's method (equations (10) and (11)) and are shown in Figure 5. The trajectories are perpendicular to the propagation time fronts, in accordance with equation (3a) and the fact that $\mathbf{p} = \nabla\sigma$. Trajectories $\mathbf{X}(r)$, such as those shown in Figure 5, form the basis of an efficient inversion scheme.

[16] We wish to emphasize that the trajectories associated with transient head variations are not equivalent to streamlines. For example, the trajectories do not depend on time, while streamlines are time-dependent quantities. To illustrate this point we compute the streamlines from observation well 11 to pumping well 9. The first streamline is associated with an early time (0.17×10^{-5} days) while the second corresponds to a later time (0.17 days). The streamlines are denoted by the solid lines in Figure 6. The corresponding trajectory for the transient problem is indicated by the dashed line in each panel. In this example, early time streamlines do appear to follow our computed trajectories. While at early times the streamline and the trajectory are similar, it is evident that the two curves differ significantly at later times (0.17 days). The streamlines, which are based upon the head gradient, are influenced by conductivity variations surrounding the array of boreholes and the initial and boundary conditions. At later times, the streamlines are increasingly sensitive to the flow properties at the edge of the grid. In contrast, the transient head trajectory is most strongly dependent upon the diffusivity between the pumping and observation wells (equations (3a) and (3b)) and the initial and boundary conditions.

2.2. Tracer Transport

[17] In this section we consider a tracer test. That is, a chemical tracer is rapidly introduced into a source well while the concentration, $c(\mathbf{x}, t)$, is measured in surrounding boreholes. The governing equation is [*Bear*, 1972; *de Marsily*, 1986, p. 240]

$$\omega_c \frac{\partial c}{\partial t} = \nabla \cdot (\mathbf{D}\nabla c - \mathbf{U}c) \tag{12}$$

where ω_c is the kinematic porosity, $\mathbf{D}(\mathbf{x})$ is the dispersion tensor, and $\mathbf{U}$ is the Darcy velocity which is given by

$$\mathbf{U} = \mathbf{K} \cdot \nabla h \tag{13}$$

where $\mathbf{K}$ is the hydraulic conductivity tensor.

[18] In Appendix A we derive an asymptotic solution to the convection-diffusion equation (12) describing solute transport. As for transient head, the solution is defined along a trajectory, or curve $\mathbf{X}(l)$, through the model. We compute the trajectory by solving the system of differential equations

$$\frac{d\mathbf{X}}{dl} = \mathbf{U} \tag{14a}$$

$$\frac{d\sigma}{dl} = \omega_c \tag{14b}$$

were l is a parameter signifying position along the trajectory and $\sigma(\mathbf{X})$ is a measure of the propagation time from the injection well to the point $\mathbf{X}$. Transforming the problem into

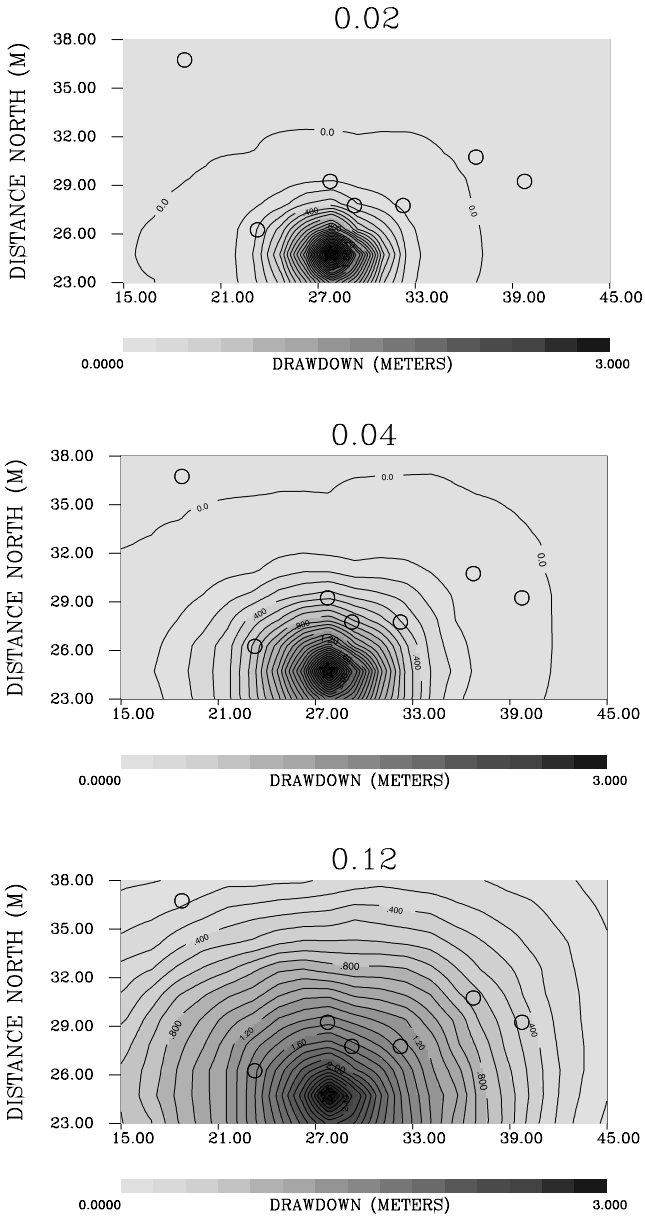

Figure 2. Calculated drawdown due to fluid withdrawal from well 9. The calculations correspond to three distinct times: 0.02, 0.04, and 0.12 $\sqrt{\text{days}}$. Well 9 is denoted by a star, and observation wells are indicated by open circles.

a coordinate system defined by **U** we obtain an integral expression for $\sigma(\mathbf{X})$

$$\sigma = \int_{\Sigma} \frac{\omega_c}{U} dr \tag{15}$$

where Σ is the trajectory from the injection well to the observation well and $U = |\mathbf{U}|$. Combining Darcy's law (13) and equation (15) results in an analytic expression for the propagation time, σ, in terms of reservoir flow properties

$$\sigma = \int_{\Sigma} \frac{\omega_c}{|\mathbf{K} \cdot \nabla h|} dr. \tag{16}$$

[19] Our calculation of the trajectory $\mathbf{X}(l)$ relies upon output from a numerical simulator. The first step in this approach is a forward simulation to compute the head, $h(\mathbf{x}, t)$. Next, the head gradient is computed by numerical differencing and projecting onto the conductivity tensor **K** to compute **U**. The trajectories are then calculated using Heun's method, as described in section 1. In Heun's method an intermediate point

$$\hat{\mathbf{X}}_i = \mathbf{X}_i - \mathbf{U}(\mathbf{X}_i)\delta r \tag{17}$$

is used to refine our estimate of **U**. The direction of the (i + 1)th step is the average of the **U** at $\mathbf{X}_i$ and **U** at the intermediate point $\hat{\mathbf{X}}_i$,

$$\mathbf{X}_{i+1} = \mathbf{X}_i - \frac{\delta r}{2}\left[\mathbf{U}(\mathbf{X}_i) + \mathbf{U}(\hat{\mathbf{X}}_i)\right]. \tag{18}$$

Using Heun's method we simply march in the direction of **U** from the observation well to the injection well.

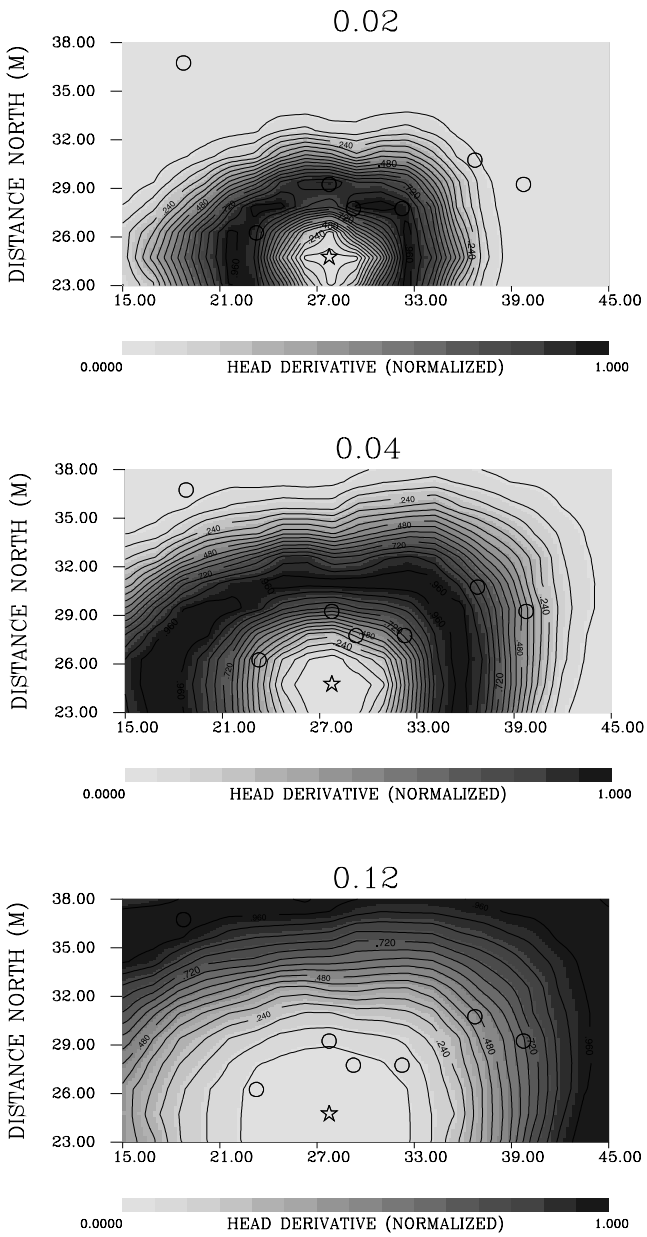

Figure 3. Normalized head time derivative, due to fluid withdrawal from well 9. The time derivative in each cell is normalized by the peak value obtained in the cell. The calculations correspond to the three distinct times of Figure 2 (0.02, 0.04, and 0.12 $\sqrt{\text{days}}$).

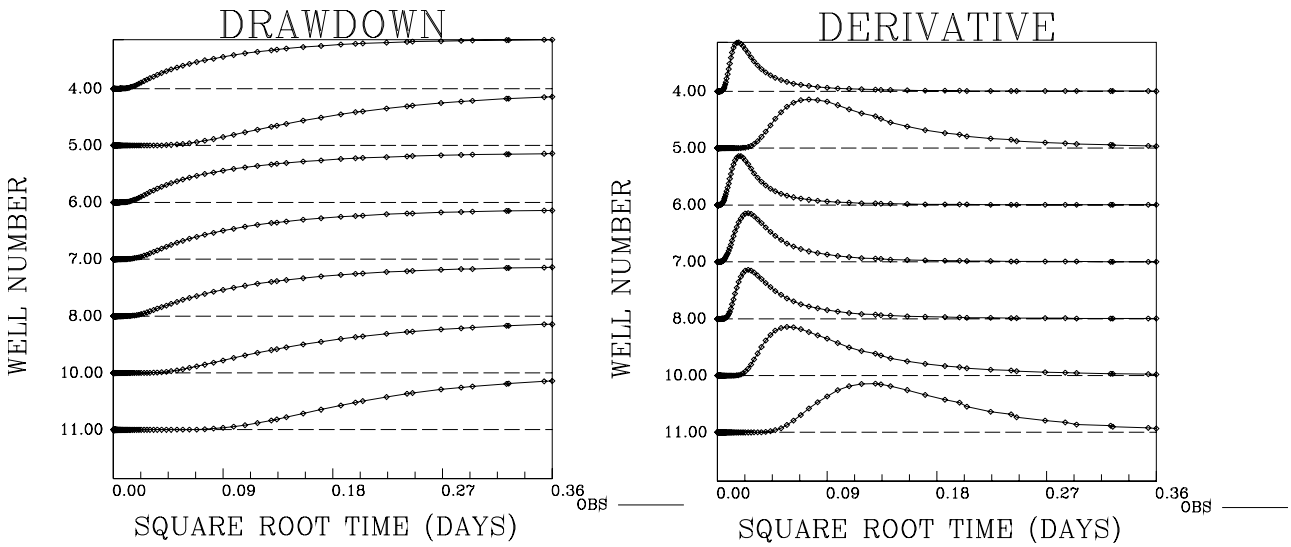

Figure 4. (left) Drawdown computed at the observation wells in Figure 1. (right) The time derivative of the computed drawdown as each of the seven observation wells.

[20] Our technique for computing trajectories for tracer transport is equivalent to defining streamlines [*Datta-Gupta and King*, 1995; *Crane and Blunt*, 1999]. In a sense, the asymptotic methodology provides a mathematical framework for streamline-based modeling of tracer transport. However, the asymptotic approach is fully general, treating the transport equation (12) which contains a dispersion tensor, **D**, and a hydraulic conductivity tensor **K**. The hydraulic head may also vary in time, as long as the variations are "slow" with respect to the appearance of the tracer, resulting in trajectories which are time-dependent. The equation governing the evolution of the tracer concentration, $c(\mathbf{X}, T)$, along the trajectory **U** is (equation (A19))

$$\omega_c \frac{\partial c}{\partial T} - \mathbf{U} \cdot \nabla c + \nabla \sigma \cdot \mathbf{D} \nabla \sigma \frac{\partial^2 c}{\partial \theta^2} = 0 \qquad (19)$$

where θ is the local "phase" and takes the form $T - \sigma(\mathbf{x})$, as noted in Appendix A. As discussed in Appendix A, equation (19) is of mixed character and is capable of modeling both diffusive as well as advective behavior, depending on the

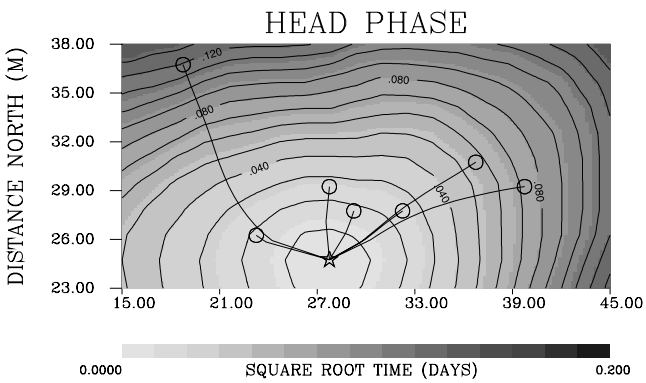

Figure 5. Contour plot of the square root of the arrival time of the peak in the head derivative. The contour units are in 0.01 days. The computed trajectories, connecting each observation well to the pumping well (9), are shown as solid lines.

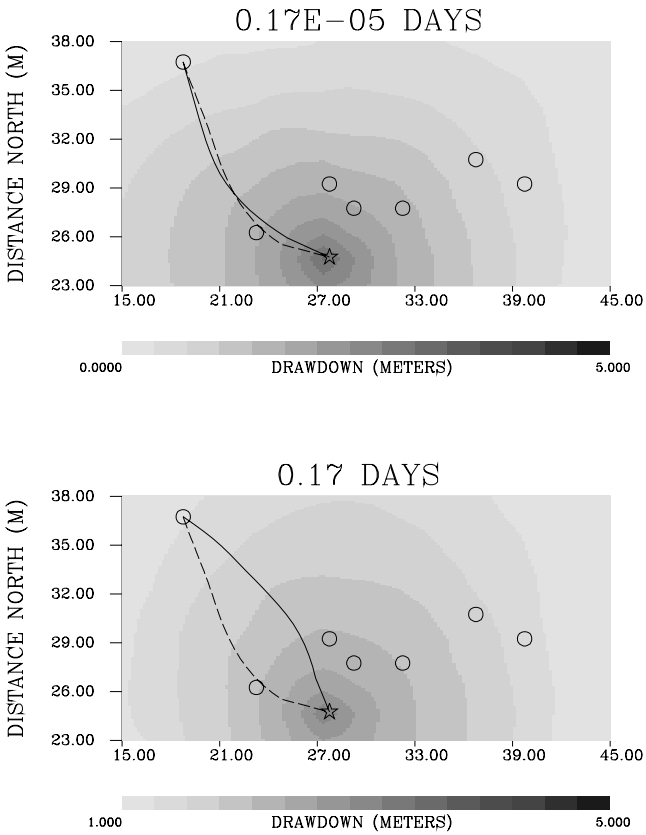

Figure 6. Streamline (solid line) and transient head (dashed line) trajectories plotted on a gray scale plot of the steady state head variation. In the top panel the streamline is computed at an early time (0.17×10^{-5} days). The streamline in the bottom panel corresponds to a later time (0.17 days).

relative size of the coefficients. For an impulsive point source of unit amplitude, equation (19) has the solution [*Carslaw and Jaeger*, 1959, p. 353]

$$c(\mathbf{X}, T) = \frac{1}{\sqrt{4\pi\tau}} \exp\left(-\frac{(T-\sigma)^2}{4\tau}\right) \tag{20}$$

where

$$\tau = \int_{\Sigma} \omega_c \frac{\nabla\sigma \cdot \mathbf{D} \cdot \nabla\sigma}{U} dr. \tag{21}$$

For a general input function we convolve the impulse response (20) with the input function.

[21] The integral (20) represents the contribution from a single trajectory Σ. Generally, as with streamlines, there will be contributions from all trajectories connecting the injection well to the observation well. If we parameterize the set of trajectories by the variable λ, such as the take-off angle, the total response at the observation well is given by the integral

$$c(\mathbf{X}, T) = \int \frac{1}{\sqrt{4\pi\tau_\lambda}} \exp\left[-\frac{(T-\sigma_\lambda)^2}{4\tau_\lambda}\right] d\lambda. \tag{22}$$

We can evaluate this integral numerically as in streamline simulation or approximate it using the method of stationary phase [*Dingle*, 1973]. The stationary phase representation is a sum over all stationary points of the argument of the exponential.

[22] We illustrate the approach using the reservoir model depicted in Figure 1. The well configuration is identical to that of a tracer test conducted by the Swiss National Cooperative for the Storage of Radioactive Waste (Nagra) described below. Tracer is injected into well 4 and extracted from well 10. We simulated 200 days of flow and transport using the TOUGH2 code [*Pruess et al.*, 1999]. Three snapshots of tracer concentration 5, 21, and 40 days, are shown in Figure 7. The concentration history at the extraction well is shown in Figure 8. From the flow field in each grid block we compute the head gradient and the corresponding vector **U**. On the basis of **U** we use equations (17) and (18) to define the trajectory from the extraction well to the injector (Figure 9). Thus in a single forward simulation we obtain the trajectory which forms the basis for an inversion of tracer data as discussed in section 2.3.

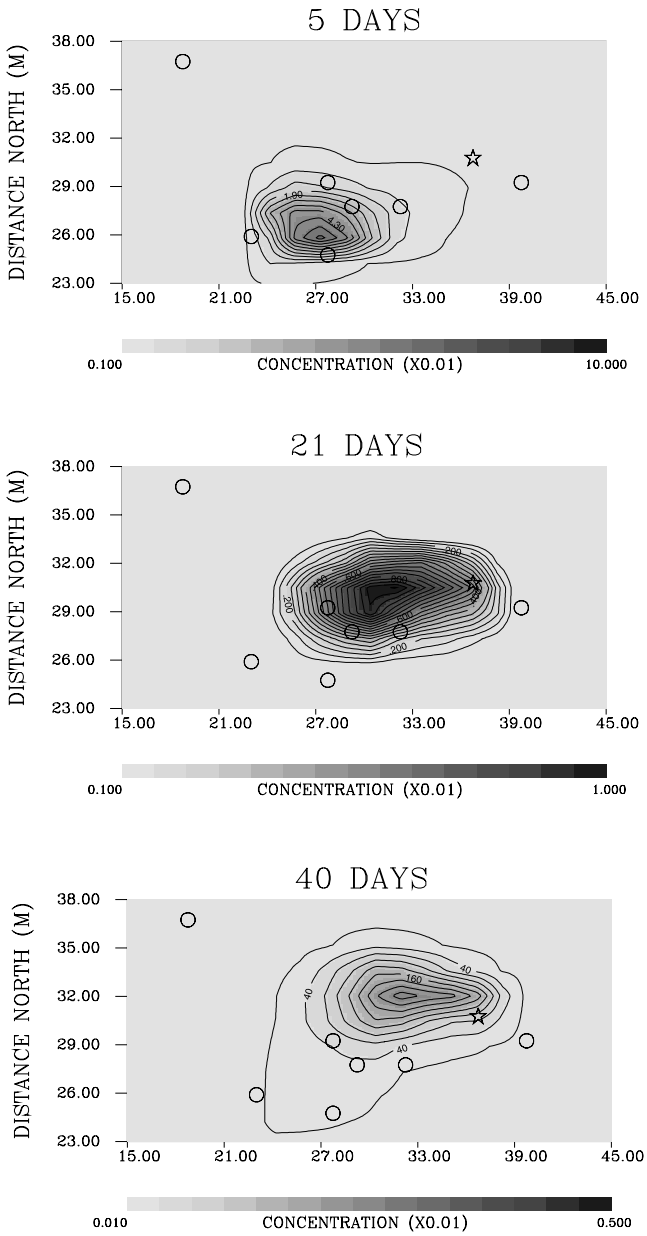

Figure 7. Solute concentrations at three times. The calculations correspond to a test in which a spike of solute is injected in well 4 while fluid is withdrawn from well 10 (denoted by a star).

2.3. An Efficient Inversion Scheme for Flow and Transport Data

[23] In this section we outline the specific algorithms used in the application. In particular, we describe the matching of head and tracer arrival times to estimate hydraulic conductivity. There is some advantage in utilizing arrival times when treating transient head and tracer observations. First, the analysis is straight-forward and equations (5) and (16) relating arrival times to flow properties, are relatively simple. Secondly, the units for the flow and transport inversions are comparable; we work in terms of the arrival time in days (tracer) or the square root of days (head). This is in contrast to amplitudes in which head may be recorded in meters and concentration may be measured in parts per million (ppm). Thirdly, the arrival time sensitivities are relatively uniform along a path connecting the active boreholes. Amplitude sensitivities, particularly those associated with head variations, are often largest at the boreholes. This reflects the fact that the amplitudes are strongly influenced by the coupling between the boreholes and the surrounding rock.

2.3.1. Head Travel Times

[24] We shall consider a constant flow rate test. That is, from an initially quiescent state, pumping begins and rapidly settles down to an essentially constant rate. The source time function is similar in form to a Heaviside (step) function. As noted above, if we consider the time derivative of head we can identify an arrival time. It is associated with the time at which the peak head slope occurs, the maximum

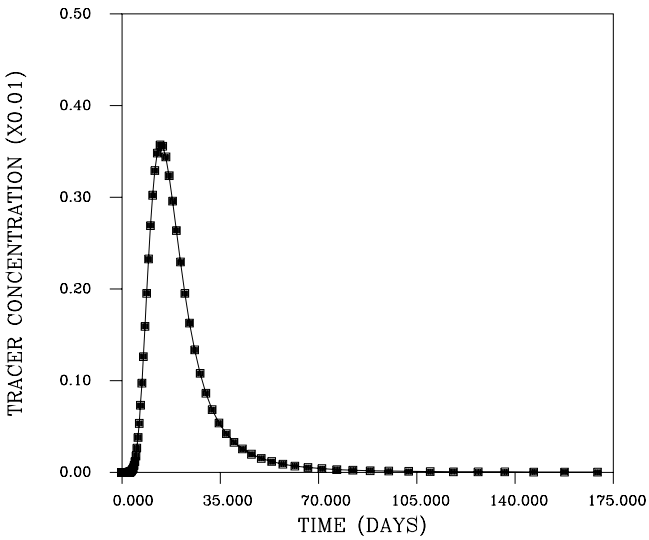

Figure 8. The tracer concentration history at well 10 for the 175 day duration of the test.

of the time derivative. The square root of the arrival time of the peak slope, T_{peak}, is given by combining equations (4), (5), and (9)

$$\sqrt{T_{peak}} = \frac{1}{\sqrt{6}} \int_{\Pi} \sqrt{\frac{S(\mathbf{X})}{K(\mathbf{X})}} dr \tag{23}$$

where $K(\mathbf{X})$ denotes the hydraulic conductivity and $S(\mathbf{X})$ denotes the storage coefficient along the path of integration, Π. The distance along the trajectory Π is parameterized by r. Using a perturbation approach we can relate a small change in hydraulic conductivity in the subsurface δK to a deviation in the calculated arrival time $\delta\sqrt{T_{peak}}$. That is, we consider background values in storage and conductivity, denoted by S_0 and K_0, respectively. We perturb the background conductivity distribution $K_0(\mathbf{X})$ by $\delta K(\mathbf{X})$, resulting in the new values $K(\mathbf{X}) = K_0(\mathbf{X}) + \delta K(\mathbf{X})$. As shown by *Vasco et al.* [2000]

$$\delta\sqrt{T_{peak}} = \frac{1}{\sqrt{6}} \int_{\Pi} \sqrt{\frac{S_0(\mathbf{X})}{K_0(\mathbf{X})}} \frac{\delta K(\mathbf{X})}{K_0(\mathbf{X})} dr. \tag{24}$$

The path of integration is a curve Π extending from the pumping well to the observation well. As described above, the integration path Π is determined from the output of a single simulation run.

[25] In order to compute model parameter sensitivities numerically we need to discretize the variations in conductivity. This can be accomplished using a basis expansion

$$\delta K(\mathbf{X}) = \sum_{l=1}^{M} \delta K_l \Upsilon_l(\mathbf{X}). \tag{25}$$

where the quantity δK_l is an expansion coefficient which we may interpret as the average conductivity perturbation in the lth block and M represents the total number of cells in the reservoir model. The basis functions $\Upsilon_l(\mathbf{y})$ are rectangular constant functions associated with a grid block-based representation. For these functions, $\Upsilon_l(\mathbf{y})$ takes the value one in the lth cell and zero outside of the lth cell. Upon substituting our representation equation (25) into the functional equation (24) we arrive at the discrete linear equation

$$\delta\sqrt{T_{max}} = \sum_{l=1}^{M} g^l \delta K_l \tag{26}$$

where

$$g^l = \int_{\Pi_l} \frac{1}{K_0(\mathbf{X})} \sqrt{\frac{S_0(\mathbf{X})}{K_0(\mathbf{X})}} dr. \tag{27}$$

Because of the nature of the basis functions $\Upsilon_l(\mathbf{x})$, which vanish outside of block l, the integral (27) is over that portion of the trajectory which lies in block l; we denote this segment by Π_l.

[26] Given a number of arrival times for a set of boreholes, equation (26) defines one of a collection of linear constraints on the conductivity perturbations. We may write this collection of linear constraints in matrix-vector form

$$\delta\mathbf{T}_h = \mathbf{G}_h \delta\mathbf{K} \tag{28}$$

where $\mathbf{G}_h$ is the matrix with coefficients equation (27), $\delta\mathbf{K}$ is a vector containing the conductivity deviations for each grid block, and $\delta\mathbf{T}_h$ is the vector of observations. Note that the linear system (28) is sparse, the only nonzero coefficients of $\mathbf{G}_h$ correspond to cells intersected by trajectories.

2.3.2. Tracer Travel Times

[27] Similar considerations apply to solute arrival times, as obtained from a tracer test. The tracer travel time, equation (16), is related to the flow properties by the integral

$$T_c = \int_{\Sigma} \frac{\omega_c(\mathbf{X})}{|K(\mathbf{X})\nabla h(\mathbf{X})|} dr \tag{29}$$

where $K(\mathbf{X})$ is the hydraulic conductivity, $\omega_c(\mathbf{X})$ is the kinematic porosity, ∇h is the head gradient, and Σ is the path of integration. Note that the path associated with the tracer transport Σ generally differs from the transient head path Π.

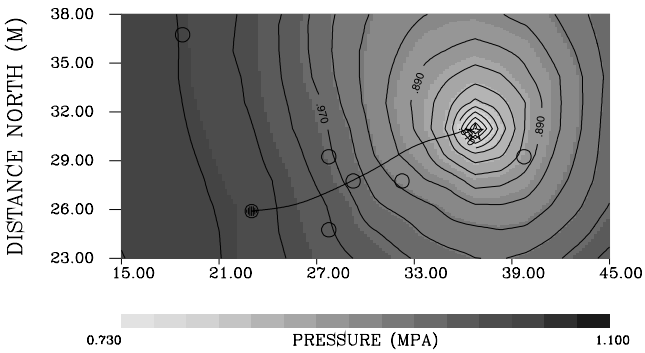

Figure 9. Steady state pressure contours associated with the tracer test. The fluid is withdrawn from well 10, which is denoted by a star. The trajectory, determined by the pressure gradient, is indicated by the solid curve.

In particular, the transient head test and tracer test are typically distinct experiments with different borehole configurations and pumping histories. For example, tracer tests are usually conducted under conditions of steady state flow. Using a perturbation approach [*Vasco and Datta-Gupta*, 1999] we can relate a small change in hydraulic conductivity to a perturbation in the solute arrival time

$$\delta T_c = \int_{\Sigma} \frac{\omega_0(\mathbf{X})}{|K_0(\mathbf{X})\nabla h_0(\mathbf{X})|} \frac{\delta K(\mathbf{X})}{K_0(\mathbf{X})} dr \tag{30}$$

for background conductivities, kinematic porosity, and head, K_0, ω_0, and h_0, respectively. Using the basis expansion (25) for hydraulic conductivity, we can write the integral (30) as the sum

$$\delta T_c = \sum_{l=1}^{M} f^l \delta K_l \tag{31}$$

where

$$f^l = \int_{\Sigma_l} \frac{1}{K_0(\mathbf{X})} \frac{\omega_0(\mathbf{X})}{|K_0(\mathbf{X})\nabla h_0(\mathbf{X})|} dr. \tag{32}$$

For a collection of arrival time observations we will have a set of equations of the form of equation (31). We may write this set of equations in matrix-vector notation

$$\delta \mathbf{T}_c = \mathbf{F}_c \delta \mathbf{K} \tag{33}$$

where the coefficients of the matrix $\mathbf{F}_c$ are given in equation (32) and $\delta\mathbf{K}$ and $\delta\mathbf{T}_c$ are the model parameter and data vectors, respectively.

2.3.3. Regularization and Solution of the Inverse Problem

[28] If we have observations from a series of pumping and tracer tests we can use these data to constrain the conductivity variations in the subsurface

$$\begin{bmatrix} \delta \mathbf{T}_h \\ \\ \delta \mathbf{T}_c \end{bmatrix} = \begin{bmatrix} \mathbf{G}_h \\ \\ \mathbf{F}_c \end{bmatrix} \delta \mathbf{K}. \tag{34}$$

Typically there are many more model parameters than there are observations and the system (34) is very much underdetermined. Thus solving the system (34) directly will produce an unstable solution which can change dramatically under any perturbation of either the data or matrix coefficients.

[29] One way to stabilize the inverse problem is to introduce some form of regularization. Regularization entails introducing penalty terms which ensure that some property of the model, such as its norm, does not grow exceedingly large. For example, given that our data are from widely separated boreholes and are not uniquely sensitive to small-scale variations in conductivity, we might expect that we can only constrain large-scale conductivity variations reliably. Thus we could introduce a regularization term which penalizes small-scale, or rough, features of our model. A measure of model roughness is provided by the norm of the vector of spatial derivatives of the model. That is, if $\mathbf{L}$ is a matrix differencing operator which differences the conductivity of adjacent cells in the reservoir model then a measure of model roughness is given by the quadratic form

$$Q_r = \| \mathbf{L}\delta\mathbf{K} \|^2 . \tag{35}$$

As shown by *Datta-Gupta et al.* [2002], if we denote the augmented coefficient matrix

$$\mathbf{\Gamma} = \begin{bmatrix} \mathbf{G}_h \\ \\ \mathbf{F}_c \\ \\ \alpha\mathbf{L} \end{bmatrix} \tag{36}$$

and the augmented data vector

$$\mathbf{T} = \begin{bmatrix} \delta\mathbf{T}_h \\ \\ \delta\mathbf{T}_c \\ \\ \mathbf{0} \end{bmatrix} \tag{37}$$

we may write the necessary equations for a regularized least squares solution as

$$\mathbf{\Gamma}^T\mathbf{\Gamma}\delta\mathbf{K} = \mathbf{\Gamma}^T\mathbf{T} \tag{38}$$

[*Parker*, 1994, p. 44]. The scalar parameter α controls the trade-off between fitting the data and obtaining a smooth model. Approaches for choosing α range from trial and error to the systematic construction of a trade-off curve [*Parker*, 1994 p. 137]. The system (38) may be solved using any linear system solver. Because of the sparsity of $\mathbf{\Gamma}$ we use the LSQR algorithm of *Paige and Saunders* [1982] which only works with the nonzero coefficients of the array. Furthermore, the algorithm consists of a number of vector-matrix multiplies applied to $\mathbf{\Gamma}$ and $\mathbf{\Gamma}^T$. To maintain efficiency, the potentially dense matrix product $\mathbf{\Gamma}^T\mathbf{\Gamma}$ is never formed.

2.3.4. Model Parameter Resolution

[30] For a fine discretization of the subsurface, large M in equations (26) and (31), the conductivity estimates for individual cells cannot be uniquely determined. Rather, only spatial averages of the property can be estimated unambiguously. A determination of the scale at which model parameter variations may be reliably estimated follows from the resolution matrix [*Tarantola*, 1987; *Parker*, 1994; *Vasco et al.*, 1997]. The functional form of the resolution matrix follows from the assumption that there exists a ''true'' model, $\delta\mathbf{K}_t$, related to the data by equation (34). However, because the system of equations (34) is ill-conditioned when M is large, it cannot be solved in a numerically stable fashion. Rather, a stable estimate of the model parameters results from solving the regularized equations (38) [*Tarantola*, 1987; *Parker*, 1994]. Because of the linearization, model parameters estimates $\delta\hat{\mathbf{K}}$ are linearly related to the observations

$$\delta\hat{\mathbf{K}} = \mathbf{\Gamma}^{\dagger}\mathbf{T} \tag{39}$$

where $\mathbf{\Gamma}^{\dagger}$ denotes the generalized inverse [*Tarantola*, 1987] used to solve equation (38) for $\delta\mathbf{K}$, which is given by

$$\mathbf{\Gamma}^{\dagger} = \left(\mathbf{\Gamma}^T\mathbf{\Gamma}\right)^{-1}\mathbf{\Gamma}^T \tag{40}$$

Substituting the expression (34) for the nonzero part of $\mathbf{T}$ into equation (38), noting that $\delta\mathbf{K}$ is our true model $\delta\mathbf{K}_t$, one arrives at

$$\delta\hat{\mathbf{K}} = \mathbf{\Gamma}^{\dagger}\begin{bmatrix}\mathbf{G}_h\\ \\ \mathbf{F}_c\end{bmatrix}\delta\mathbf{K}_t \tag{41}$$

or

$$\delta\hat{\mathbf{K}} = \mathbf{R}\delta\mathbf{K}_t \tag{42}$$

where $\mathbf{R}$ is the resolution matrix relating our estimates to the hypothetical true model. An efficient method for calculating $\mathbf{R}$ when the sensitivity matrices are sparse is given by *Datta-Gupta et al.* [2002].

[31] The resolution matrix may be thought of as a linear filter through which the actual spatial distribution of flow properties is imaged. The rows of the resolution matrix are averaging coefficients indicating the contribution of all other parameters to an estimate for a given cell. In the ideal case the resolution matrix would be an identity matrix and the properties of individual cells are perfectly resolved. In such a case there is no tradeoff with estimates for adjacent cells. One advantage of the resolution matrix is that it is independent of the data uncertainty and only depends on our model parameter sensitivities and the geometry of our experiment.

3. Application

3.1. Migration Experiment, Switzerland

[32] In this section we apply the inverse method to data from the Grimsel Rock Laboratory in Switzerland. The Grimsel facility is located within the Bernese Alps and consists of a series of tunnels and boreholes lying a few hundred meters below the surface [*Mauldon et al.*, 1993]. Numerous pressure and tracer tests have been conducted at the facility, providing a wealth of observations for fracture zone characterization. To date, the transient pressure observations have been used to characterize the conductivity of fractures within the subsurface [*Mauldon et al.*, 1993; *Vasco et al.*, 1997]. In this section we shall examine both head and tracer observations in an effort to further constrain the fracture zone heterogeneity.

3.2. Background

[33] Our data set consists of observations from pressure and tracer tests conducted in a northeast striking fracture zone. The zone dips steeply (78°) to the southeast and is relatively isolated from surrounding fractures and faults. The fracture zone, known as the Migration or MI fracture zone, consists of a series of subparallel braided fractures roughly half a meter in thickness. Conductivity within the fracture zone is variable and is influenced by the distribution of mylonite, cataclasite, and other gouge materials present in the subfractures [*Mauldon et al.*, 1993]. The fracture zone is intersected by an access tunnel and two laboratory tunnels in the vicinity of the experiments. The two laboratory tunnels are far enough from the experiment that we can neglect their effects. The access tunnel is modeled as a constant pressure boundary condition [*Mauldon et al.*, 1993]. Eight boreholes, drilled from the laboratory tunnel, intersect the MI fracture zone in a tightly spaced array (Figure 1). The borehole intervals intersecting the fracture zone are isolated by packers.

3.3. Hydrologic Tests

[34] Two groups of constant head and constant rate tests were conducted at the MI site and these tests have been discussed elsewhere [*Solexperts*, 1989; *Davey et al.*, 1989; *Mauldon et al.*, 1993]. Here we utilize observations from a test conducted at the end of 1988 involving a constant fluid withdrawal of 340 mL/min [*Vasco et al.*, 1997] from borehole 9. Our approach to the analysis of these data will be quite different from previous studies [*Mauldon et al.*, 1993; *Vasco et al.*, 1997]. In particular, we shall work with arrival times, using equation (5), rather than directly with head or pressure variations. This approach complements the previous studies and we shall be able to compare our resulting models with those of *Mauldon et al.* [1993] and *Vasco et al.* [1997]. In order to estimate travel times to the surrounding boreholes, consider the time derivative of the pressure variations (Figure 10). Because the experiments were not designed to accurately measure the peak slope, the time sampling is not optimal for this task. In particular, for boreholes 4 and 6 the peak slope occurs at the second sample point (Figure 10). Still, we are able to recover the peak arrival time at each borehole to within the sampling interval. Note the great variation in slopes across the array of boreholes, both in amplitude and arrival time. Some of the variation is undoubtedly due to the varying distances of the boreholes from the pumping well but there may also be some influence from conductivity heterogeneity.

[35] A series of dipole tracer tests were conducted using various well pairs. We shall consider observations from dipole tests involving boreholes 4 and 10, a distance of roughly 14 meters. A conservative Uranine tracer solution was injected into borehole 4 at a flow rate of 8 mL/min [*Vasco et al.*, 1997]. The flow rate in extraction borehole 10 was 120 mL/min. The tracer entering the low volume packed-off injection interval was measured by a downhole laser optrode instrument [*Fierz*, 1993]. Injection and extraction pressures and Uranine concentrations were recorded every 5 min. The experiment was conducted for 370 hours before the injection pump failed [*Fierz*, 1993]. However, Uranine breakthrough occurred before the end of the first day (Figure 11). One peak is evident in the concentration history. Concentration profiles of other injected tracers, iodine and helium, displayed similar arrival times [*Fierz*, 1993]. Furthermore, a repeat experiment, utilizing nearly identical flow rates, produced essentially the same breakthrough times. Thus the tracer results, particularly the breakthrough times, appear to be quite robust.

3.4. Inversion of Head and Tracer Observations

[36] We have complementary transient head and steady state tracer travel time observations. It is evident from equations (5) and (16) that these data are sensitive to hydraulic conductivity variations. Thus it makes sense to

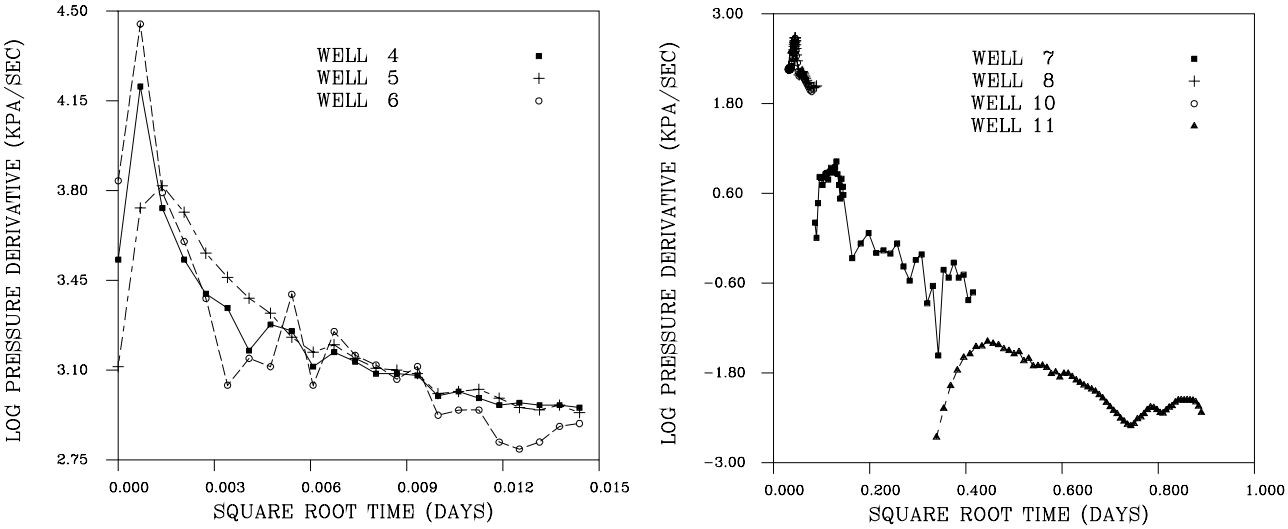

Figure 10. The time derivative of the transient pressure observations from the Migration (MI) experiment. The values are plotted on a logarithmic scale, and the horizontal scale is the square root of time.

use tracer and head arrival times to constrain the flow properties of the fracture zone. However, before we embark on this task there are some issues which need to be addressed. First, head arrival times depend on the storage coefficient S while the tracer is dependent on the kinematic porosity ω_c. These quantities most likely differ, perhaps significantly, and we need to estimate the relative sizes of these parameters. Secondly, in combining two different classes of observations, head and tracer, we must decide how to weigh each data constraint in the inversion.

[37] In our study we assume the storage coefficient S within the fracture zone is uniform. Thus we shall be mapping variation in S into our estimates of hydraulic conductivity K. As noted by *Vasco and Karasaki* [2001], it is possible to invert for both S and K using transient head observations. Specifically, the low-frequency component of head change is controlled by the hydraulic conductivity. Conversely, the high-frequency component of head variation is primarily sensitive to the coefficient of storage. However, using only arrival times it is not possible to distinguish between variations in S and K, as indicated by equations (4) and (5). The background storage coefficient was set to a value of 5.7×10^{-7}, based upon past studies of transient and steady state head data at the MI fracture zone [*Mauldon et al.*, 1993; *Vasco et al.*, 1997].

[38] In order determine the relative size of ω_c and S, we took an inversion result in which we simply matched the transient head arrival times and used it to simulate the tracer experiment conducted at the MI fracture zone. We found that the predicted tracer arrival time was too large by a significant factor. The kinematic porosity was systematically lowered in a series of simulations until the arrival time magnitude roughly agreed with the observed value of 0.54 days. The estimate of ω_c was 0.01, which was fixed in the subsequent joint inversion.

[39] The relative weighting of tracer and head constraints is based upon the estimated standard errors of each observation. That is, we normalize each data constraint by its estimated standard error. The arrival time error estimates are based upon the sampling intervals for the head and tracer time series. Specifically, one-half of the sampling interval is taken as the estimated arrival time error. This is a relatively simple estimate to calculate. We could have made use of more sophisticated error models which accounted for possible clock errors. For our illustrative purposes the sampling interval error estimates are adequate.

[40] Our starting model is uniform, with a constant background hydraulic conductivity of 2.2×10^{-13} m^2. At each step of the inversion algorithm we simulate both the pump and the tracer tests. Thus two simulations are required to compute the residuals and trajectories necessary for an inversion step. However, this is the minimum number of simulations required by any inversion algorithm. In total, 30 iterations were required to reduce both the head and

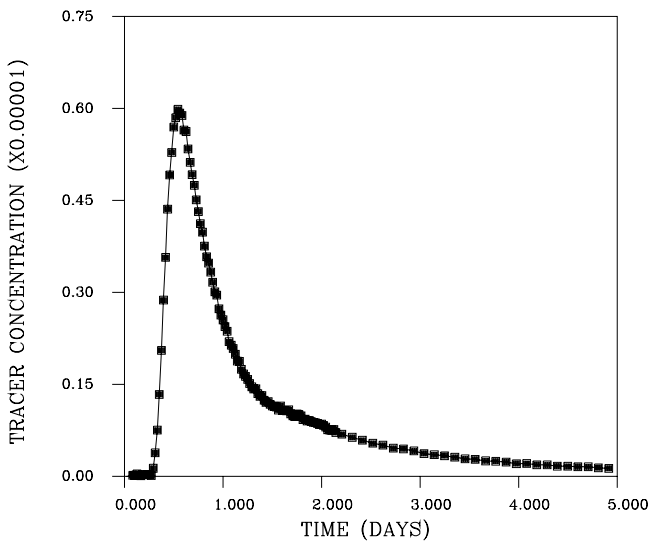

Figure 11. Uranine concentration history associated with a dipole tracer test involving borehole 4 (injection) and borehole 10 (extraction).

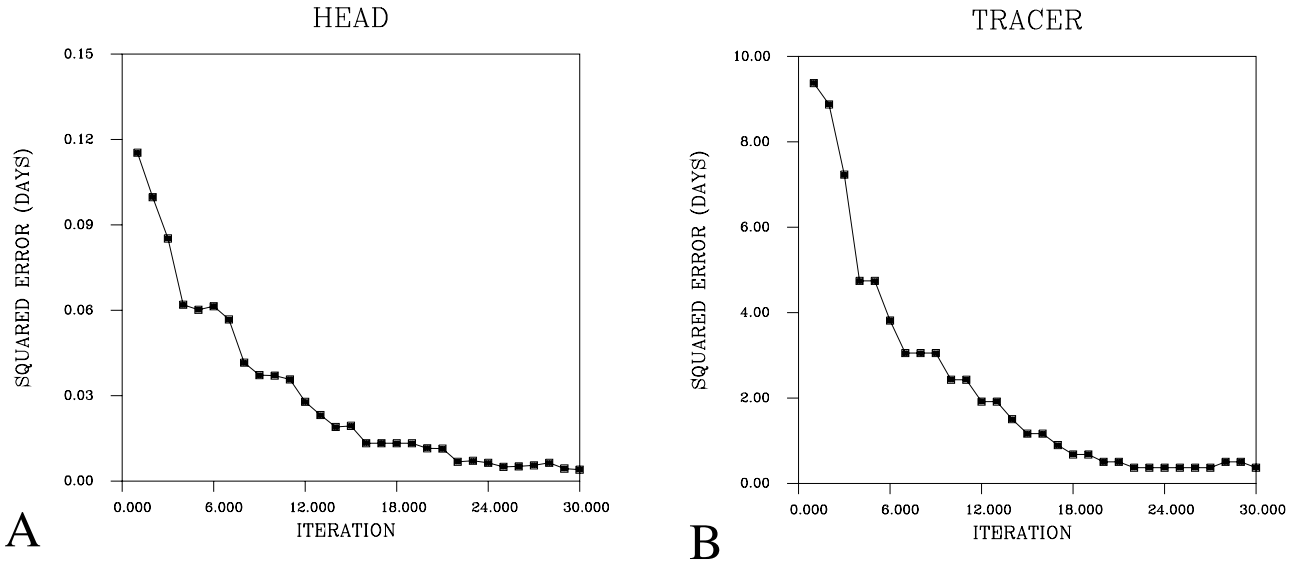

Figure 12. Arrival time misfits for both head and tracer observations. These curves correspond to a simultaneous inversion of the head and tracer data.

tracer misfits by over an order of magnitude (Figure 12). Thus for the simultaneous inversion of head and tracer observations a total of 60 numerical simulations are necessary. This compares quite favorably with the 96,001 simulations which would be required for a straight-forward gradient-based inversion algorithm. Both the head and tracer arrival time error reductions flatten out after about 25 iterations. By the final iteration the fit to both the head and tracer arrival times is fairly good (Figure 13).

[41] The model of hydraulic conductivity variation in the MI fracture zone, compatible with both the head and tracer arrival time observations, is shown in Figure 14. We observed a high-conductivity channel curving from borehole 4 to borehole 5. In addition, there is a band of low conductivity just above the high-conductivity channel. Our results are very similar to those of *Vasco et al.* [1997] and *Davey et al.* [1989] which are based upon head amplitude inversions.

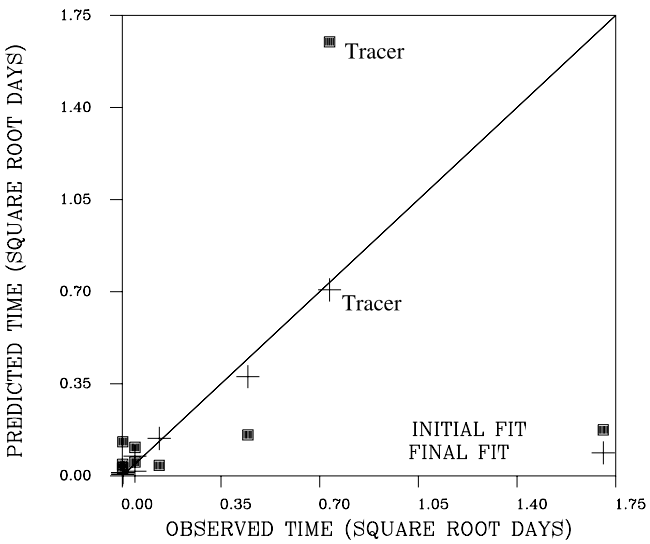

Figure 13. Initial (solid squares) and final (crosses) fits to the head and tracer arrival times. The fits are associated with a simultaneous inversion of head and tracer arrival times. The two points, initial and final fits for the tracer arrival, are labeled TRACER.

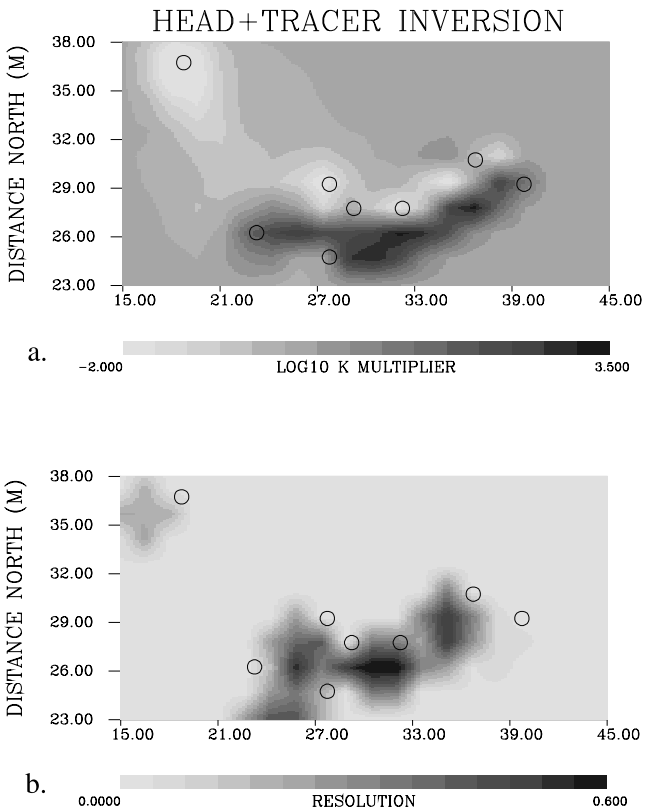

Figure 14. (a) Hydraulic conductivity estimates resulting from a simultaneous inversion of head and tracer arrival times. (b) Diagonal elements of the model parameter resolution matrix. Poorly resolved cells have values close to zero, and well-resolved cells are close to unity.

[42] We end this section with a discussion on the resolution of hydraulic conductivity variations in the MI fracture zone. Using equations (40) and (41) we calculate the diagonal elements of the model parameter resolution matrix **R** (Figure 14). Values close to unity indicate one may estimate the particular parameter with little interference from other parameters [*Vasco et al.*, 1997]. Values close to zero mean that there is considerable trade-off between the estimate of the parameter and the value of other model parameters. Resolution estimates depend on a local linearization about the final model parameter estimates. Because of the nonlinearity of the inverse problem, the model parameter sensitivities which enter into the resolution calculations are a function of the final conductivity model. The well resolved cells are located between the boreholes where one or more trajectories constrain the conductivities. It should be noted that the resolution resulting from an inversion of arrival times is very different from model parameter resolution associated with an amplitude inversion [*Vasco et al.*, 1997]. This is most likely due to the differences in the amplitude and arrival time sensitivities. For a uniform medium, head arrival time sensitivities are uniform along the trajectories. On the other hand, head amplitude sensitivities are strongly influenced by conductivity variations near the boreholes, particularly for later times [*Vasco et al.*, 1997]. Thus many of the well resolved cells noted by *Vasco et al.* [1997] are associated with observation boreholes. Another factor influencing the resolution may be the differences between our final models. The amplitude inversion of *Vasco et al.* [1997] contains an extremely low conductivity barrier to flow. Because the arrival time sensitivities depend on the inverse of conductivity, as in equation (6), the resolution will also depend on the magnitude of conductivity in each cell.

4. Conclusions

[43] Given the considerable computation associated with numerical simulation it is desirable to have inverse methods which do not require much additional overhead. In this paper we have developed a trajectory-based inversion scheme which is efficient yet easy to implement. As such, our approach is similar to techniques used with great success in medical imaging [*Arridge*, 1999] and geophysical tomography [*Iyer and Hirahara*, 1993]. Our derivation of the asymptotic solution for tracer transport was fairly extensive. Our aim was to show that asymptotic methods are applicable to the general equations governing head and solute evolution in a heterogeneous porous medium. In practice, the implementation of the methodology is relatively simple. The entire procedure for defining a trajectory can be accomplished in a hundred or so lines of computer code.

[44] The asymptotic approach has some useful aspects that provide additional flexibility. For example, the inverse problem is partitioned into arrival time matching and amplitude matching. To date, the arrival time matching problem has received scant attention in the literature. However, working with head arrival times has some advantages over steady state amplitudes. The peak slope is recorded much earlier than is the steady state head amplitude. Thus pumping tests relying on arrival times can be conducted much more quickly than conventional tests. The reduced time required for such tests makes cross-well pressure tomography a real possibility [*Karasaki et al.*, 2000; *Vasco and Karasaki*, 2001].

[45] The trajectory-based inverse method described here scales well with problem size. Because the model parameter sensitivities are defined along trajectories through a reservoir model, the level of computation scales roughly as the cube root of the size of a three-dimensional problem. That is, if one doubles the number of cells in each direction of a reservoir model, the total number of grid blocks will grow by 2^3 while the number of cells encountered by a trajectory will only increase by 2. Because there are sparse matrix inverse techniques which only consider cells with nonzero sensitivity, the amount of computation is limited to the cells intersected by the particular trajectories. Thus the amount of computation associated with solving the inverse problem scales more slowly than does the computation required to solve the forward problem.

[46] In this study we have concentrated on using arrival times to estimate variations in hydraulic conductivity. This is by no means a limitation of the methods presented here. Trajectory-based asymptotic methods are applicable to amplitudes as well as arrival times [*Vasco and Datta-Gupta*, 1999; *Vasco et al.*, 2000]. As discussed by *Vasco and Karasaki* [2001], it is possible to invert for both S and K using transient head amplitude data. Specifically, the low frequency component of head change is dominated by hydraulic conductivity. Conversely, the high-frequency component of head variation is primarily sensitive to the storage coefficient. Our intent in this study was to keep the presentation as simple as possible and to emphasize the utility of arrival times in general. In our experience [*Vasco and Datta-Gupta*, 1999; *Vasco et al.*, 2000], the inversion of arrival times is an essential prerequisite to amplitude matching. That is, in initially matching the arrival times we obtain a model of flow properties which we can then use as a starting model in the amplitude inversion. We have found that the inversion of amplitudes is more sensitive to the starting model and prone to converge to a local minimum. Furthermore, amplitude inversion typically involves more computation than does arrival time inversion. Thus rapid convergence is critical when treating amplitudes. We should point out that, even though only arrival times were used, our results contain the same large-scale features obtained when inverting transient head amplitudes directly [*Davey et al.*, 1989; *Vasco et al.*, 1997]. Thus transient head and tracer arrival times appear to contain important constraints on flow properties.

Appendix A: An Asymptotic Solution for Tracer Transport

[47] In Appendix A we derive an asymptotic solution to the general convection-diffusion equation describing solute transport (equation (12)). There are several ways to derive an asymptotic solution to this differential equation. An approach based upon the Fourier transform is perhaps the most direct and hence is quite common. However, a derivation based upon the perturbation-reduction method has some advantages over frequency domain techniques. First, the technique is applicable to nonlinear, diffusive, and dispersive phenomena [*Jeffrey and Taniuti*, 1964; *Whitham*, 1974; *Barenblatt*, 1979; *Smith*, 1981; *Jeffrey and Kawahara*, 1982; *Anile et al.*, 1993; *Grindrod*, 1996;

Knessl and Keller, 1997; *Chapman et al.*, 1999; *Vasco and Datta-Gupta*, 2001] and thus very general. For example, the method may be used in the analysis of multiphase flow data [*Vasco and Datta-Gupta*, 2001]. Second, the formalism is related to singular perturbation techniques and boundary layer methods [*Georgescu*, 1995] which are used in fluid mechanics and hydrology [*Gelhar and Collins*, 1971; *Wallach and Parlange*, 2000].

[48] In the perturbation-reduction method we assume that the concentration variations corresponding to the well test are much more rapid, both in space and time, than are variations in the background concentration. Typically, the background concentration of tracer is assumed to be negligible. If we denote the scale associated with the background concentration by L and the scale of variation in the concentration associated with the tracer test by l, we are assuming that $L \gg l$. We represent the ratio l/L by the dimensionless parameter ϵ and note that $0 < \epsilon \ll 1$. We may define slow variables, in both space and time, in terms of the parameter ϵ

$$X^i = \epsilon^2 x^i \qquad T = \epsilon^2 t. \tag{A1}$$

The relationship between the slow and fast variables involves the square of ϵ. Use of these particular time and space scales is necessary if we are to balance the effects of advection or propagation against the effects of dispersion and diffusion [*Anile et al.*, 1993]. This generalization in scaling, which allows us to apply asymptotic methods to dispersive and diffusive phenomena, was introduced by *Gardner and Morikawa* [1960].

[49] Many of the ideas developed in the perturbation-reduction method, and the related method of multiple scales [*Anile et al.*, 1993], correspond to quantities associated with a propagating wave or front. Indeed, locally we shall treat the concentration variation much like a propagating wave front. As such, we shall consider such quantities as amplitude, wave number, frequency, and phase of the front. Particularly important quantities are the amplitude and phase of the propagating concentration variation. The local phase θ is a fast or rapidly varying quantity which we define in terms of a slowly varying quantity, the phase function $\varphi(\mathbf{X}, T)$

$$\theta = \frac{\varphi(\mathbf{X}, T)}{\epsilon} = \frac{\varphi(\epsilon^2 \mathbf{x}, \epsilon^2 t)}{\epsilon}. \tag{A2}$$

[50] Formally, an asymptotic solution of equation (12) is a power series expansion in terms of the scale parameter ϵ

$$c(\mathbf{X}, T) = c_0(\mathbf{X}, T) + \sum_{n=1}^{\infty} \epsilon^n c_n(\mathbf{X}, T, \theta) \tag{A3}$$

where $c_0(\mathbf{X}, T)$ is a background concentration which is assumed to vary slowly in space and time. In what follows, we shall assume that the background concentration $c_0(\mathbf{X}, T)$ is essentially constant. The unknown quantities in equation (A3), the coefficients $\theta(\mathbf{X}, T)$ and $c_n(\mathbf{X}, T)$, are determined by substituting the series into the governing equation for concentration (12) and considering terms of various orders in ϵ. We shall be particularly interested in the low-order components in ϵ, which dominate for a rapidly varying concentration. Before substituting the series (A3) into equation (12) we note that the partial derivative operators in equation (12) may be represented in terms of derivatives with respect to the slow variables $\mathbf{X}$ and T and the phase θ

$$\frac{\partial}{\partial x^l} = \epsilon^2 \frac{\partial}{\partial X^l} + \epsilon \frac{\partial \varphi}{\partial X^l} \frac{\partial}{\partial \theta} \qquad \frac{\partial}{\partial t} = \epsilon^2 \frac{\partial}{\partial T} + \epsilon \frac{\partial \varphi}{\partial T} \frac{\partial}{\partial \theta}. \tag{A4}$$

Hence the temporal derivative in equation (12) takes the form

$$\frac{\partial c}{\partial t} = \epsilon^2 \frac{\partial c}{\partial T} + \epsilon \frac{\partial \varphi}{\partial T} \frac{\partial c}{\partial \theta}. \tag{A5}$$

Similar expressions are obtained for the spatial derivatives contained in the gradient operator as applied to $c(\mathbf{X}, T)$, $\mathbf{U}$ and $\mathbf{D}$

$$\frac{\partial c}{\partial x^i} = \epsilon^2 \frac{\partial c}{\partial X^i} + \epsilon \frac{\partial \varphi}{\partial X^i} \frac{\partial c}{\partial \theta} \tag{A6}$$

$$\frac{\partial \mathbf{U}}{\partial x^i} = \epsilon^2 \frac{\partial \mathbf{U}}{\partial X^i} \tag{A7}$$

and

$$\frac{\partial \mathbf{D}}{\partial x^i} = \epsilon^2 \frac{\partial \mathbf{D}}{\partial X^i} \tag{A8}$$

respectively. Higher-order spatial derivatives are obtained by successive applications of equation (A6). If we write equation (12) in terms of $c(\mathbf{X}, T, \theta)$ and derivatives with respect to X^i, T, and θ we have

$$\begin{aligned} \omega_c \epsilon^2 \frac{\partial c}{\partial T} + \omega_c \epsilon \frac{\partial \varphi}{\partial T} \frac{\partial c}{\partial \theta} = {} & \epsilon^4 \nabla \cdot (\mathbf{D} \nabla c) + \epsilon^4 \mathbf{D} \nabla \cdot \nabla c - \epsilon^4 \nabla \cdot \mathbf{U} c \\ & + \epsilon^3 \nabla \cdot \left(\mathbf{D} \nabla \varphi \frac{\partial c}{\partial \theta} \right) + \epsilon^3 \nabla \varphi \cdot \left(\mathbf{D} \nabla \frac{\partial c}{\partial \theta} \right) \\ & - \epsilon^2 \mathbf{U} \cdot \nabla c + \epsilon^2 \nabla \varphi \cdot \mathbf{D} \nabla \varphi \frac{\partial^2 c}{\partial \theta^2} \\ & - \epsilon \nabla \varphi \cdot \mathbf{U} \frac{\partial c}{\partial \theta}. \end{aligned} \tag{A9}$$

A1. Terms of Order ϵ: An Equation for the Phase

[51] Substituting the asymptotic series (A3) into equation (A9) we find, to first order in ϵ,

$$\left[\omega_c \frac{\partial \varphi}{\partial T} + \nabla \varphi \cdot \mathbf{U} \right] \frac{\partial c_1}{\partial \theta} = 0. \tag{A10}$$

Assuming that the first order approximation to the concentration amplitude, $c_1(\mathbf{X}, T, \theta)$, does not identically vanish, we arrive at the condition on φ

$$\omega_c \frac{\partial \varphi}{\partial T} + \nabla \varphi \cdot \mathbf{U} = 0. \tag{A11}$$

Using the implicit function theorem we may write equation (A11) in the form $\varphi(\mathbf{X}, T) = T - \sigma(\mathbf{X})$ where σ

only depends on position [*Kline and Kay*, 1979]. Then equation (A11) reduces to

$$\nabla\sigma \cdot \mathbf{U} = \omega_c \tag{A12}$$

a first-order linear partial differential equation, governing the distribution of the phase. We may solve this equation directly, using the method of characteristics [*Courant and Hilbert*, 1962, p. 70]. In the method of characteristics, solutions are developed along particular trajectories, the characteristic curves. We denote the characteristic curves by $\mathbf{X}(l)$, where l is a parameter signifying position along the curve. The equations for the characteristic curves are a set of ordinary differential equations

$$\frac{d\mathbf{X}}{dl} = \mathbf{U} \tag{A13}$$

$$\frac{d\sigma}{dl} = \omega_c \tag{A14}$$

[*Courant and Hilbert*, 1962, p. 70]. For a coordinate system with one axis oriented along $\mathbf{U}$ we can write equation (A13) as

$$\frac{dr}{dl} = U \tag{A15}$$

where $U = |\mathbf{U}|$ and r denotes the distance along the axis aligned with $\mathbf{U}$. Combining equations (A13) and (A14), we may write the propagation time σ as an integral

$$\sigma = \int_{\Sigma} \frac{\omega_c}{U} dr \tag{A16}$$

where Σ is the trajectory from the injection well to the observation well. Note that this expression for phase is similar to that of *Vasco and Datta-Gupta* [1999]. If we incorporate Darcy's law $\mathbf{U} = \mathbf{K} \cdot \nabla h$, equation (A16) becomes

$$\sigma = \int_{\Sigma} \frac{\omega_c}{|\mathbf{K} \cdot \nabla h|} dr. \tag{A17}$$

Note that the integral depends on time through the time dependence of the head gradient. Also, for a general conductivity tensor $\mathbf{K}$, the trajectory is not necessarily aligned with the head gradient. Rather, the trajectory follows the vector projection of the head gradient onto the conductivity tensor. For most tracer tests the head field has reached steady state or is maintained near steady state so that we can neglect the time variation. As noted by *Gelhar and Collins* [1971], equation (A11) describes the evolution of a hypothetical front or discontinuity in tracer concentration which would be realized if no dispersion or diffusion occurred. It is about this front that the tracer is dispersed and diffused. Note that if the head gradient is zero in equation (A11) the front position does not change in time.

A2. Terms of Order ϵ^2: An Equation for the Amplitude

[52] If we consider terms of order ϵ^2 in equation (A9) we obtain the following expression

$$\omega_c \frac{\partial c_1}{\partial T} + \omega_c \frac{\partial \varphi}{\partial T}\frac{\partial c_2}{\partial \theta} = -\mathbf{U} \cdot \nabla c_1 + \nabla\varphi \cdot \mathbf{D}\nabla\varphi \frac{\partial^2 c_1}{\partial \theta^2} - \nabla\varphi \cdot \mathbf{U}\frac{\partial c_2}{\partial \theta} \tag{A18}$$

containing amplitude coefficients c_1 and c_2 of the expansion (A3). However, because the phase satisfies equation (A11), terms containing c_2 drop out and we are left with

$$\omega_c \frac{\partial c_1}{\partial T} + \mathbf{U} \cdot \nabla c_1 - \nabla\sigma \cdot \mathbf{D}\nabla\sigma \frac{\partial^2 c_1}{\partial \theta^2} = 0 \tag{A19}$$

an equation for the amplitude coefficient $c_1(\mathbf{X}, T, \theta)$, accurate to order ϵ^2.

[53] We can better appreciate the range of possible behavior of $c_1(\mathbf{X}, T)$ in equation (A19) if we consider the structure of the matrix $\mathbf{D}$ in more detail. Because the matrix $\mathbf{D}$ is real and symmetric, it may be decomposed into the matrix product

$$\mathbf{D} = \mathbf{O}^t \Lambda \mathbf{O} \tag{A20}$$

where $\mathbf{O}$ is an orthogonal or rotation matrix and $\mathbf{\Lambda}$ is a diagonal matrix of the form

$$\Lambda = \begin{pmatrix} \omega d + \alpha_l U & 0 & 0 \\ 0 & \omega d + \alpha_t U & 0 \\ 0 & 0 & \omega d + \alpha_t U \end{pmatrix} \tag{A21}$$

[*de Marsily*, 1986, p. 236]. Thus the dispersion matrix depends upon the total porosity ω, the molecular diffusion coefficient d, the magnitude of the Darcy velocity U, and the longitudinal and transverse dispersion coefficients, α_l and α_t, respectively. If the flow velocity is weak or zero, equation (A19) reduces to a pure diffusion equation

$$\omega_c \frac{\partial c_1}{\partial T} - \omega d \nabla\sigma \cdot \nabla\sigma \frac{\partial^2 c_1}{\partial \theta^2} = 0. \tag{A22}$$

On the other hand, if the molecular diffusion and dispersion coefficients are very small the result is the equation describing pure advective transport

$$\omega_c \frac{\partial c_1}{\partial T} + \mathbf{U} \cdot \nabla c_1 = 0. \tag{A23}$$

Generally, the nature of the transport will lie somewhere between these extremes.

[54] We can consider the coefficient $\nabla\sigma \cdot \mathbf{D}\nabla\sigma$ in equation (A19) to be a quadratic form. By a theorem of linear algebra [*Noble and Daniel*, 1977, p. 420], this quadratic form is equivalent to

$$Q(\mathbf{X}) = (\omega d + \alpha_l U) y_1^2 + (\omega d + \alpha_t U) y_2^2 + (\omega d + \alpha_t U) y_3^2 \tag{A24}$$

where

$$\mathbf{y} = \mathbf{O}^t \nabla\sigma \tag{A25}$$

and $\mathbf{O}$ is the orthogonal matrix in equation (A20). We may write equation (A19) in terms of $Q(\mathbf{X})$

$$\omega_c \frac{\partial c_1}{\partial T} + \mathbf{U} \cdot \nabla c_1 - Q(\mathbf{X}) \frac{\partial^2 c_1}{\partial \theta^2} = 0. \tag{A26}$$

Writing equation (A26) in characteristic coordinates, given by equations (A13) and (A16), we arrive at

$$\frac{\partial c_1}{\partial \sigma} - Q(r)\frac{\partial^2 c_1}{\partial \theta^2} = 0 \tag{A27}$$

where r is the position along the trajectory. Like *Gelhar and Collins* [1971] we may define the integral

$$\tau = -\int_{\Sigma} Q(r)d\sigma \tag{A28}$$

or, because $d\sigma = \omega_c/Udr$

$$\tau = -\int_{\Sigma} \frac{\omega_c Q(r)}{U} dr. \tag{A29}$$

Writing equation (A26) in terms of τ produces the heat equation

$$\frac{\partial c_1}{\partial \tau} + \frac{\partial^2 c_1}{\partial \theta^2} = 0. \tag{A30}$$

For an impulsive point source of unit amplitude, equation (A29) has the solution [*Carslaw and Jaeger*, 1959, p. 353]

$$C(\mathbf{X}, T) = \frac{1}{\sqrt{4\pi\tau}} \exp\left(-\frac{(T-\sigma)^2}{4\tau}\right). \tag{A31}$$

For a general time-varying injection, we convolve equation (A31) with the particular source time function.

[55] Solution (A31) represents the contribution from a single trajectory Σ. The total tracer response is obtained by summing over all trajectories from the injection well to the observation well. That is, equation (A31) signifies the contribution from a single trajectory Σ between the boreholes. For the total response at an observation well we must integrate the responses over all contributing trajectories. It we parameterize the trajectories by a variable λ the total response is given by the integral

$$c(\mathbf{X}, T) = \int \frac{1}{\sqrt{4\pi\tau_\lambda}} \exp\left[-\frac{(T-\sigma_\lambda)^2}{4\tau_\lambda}\right] d\lambda. \tag{A32}$$

The variable λ may represent the angle at which the trajectory leaves the observation well. Furthermore, it may be a vector variable in three-dimensions, signifying two angles, or an angle and position along the well bore, necessary to specify a trajectory uniquely.

[56] As a final comment, we note that when we neglect transverse dispersion (set α_t to zero) equation (A29) reduces to the expression obtained by *Gelhar and Collins* [1971]. In this situation, equations (A24) and (A25) give

$$Q(\mathbf{X}) = (\omega d + \alpha_l U)|\nabla\sigma|^2 \tag{A33}$$

or, using equation (A10) and the fact that our coordinate system is oriented along $\mathbf{U}$

$$Q(\mathbf{X}) = {\omega_c}^2 \frac{(\omega d + \alpha_l U)}{U^2}. \tag{A34}$$

Thus equation (A29) takes a form

$$\tau = -\int_{\Sigma} \omega_c^3 \frac{(\omega d + \alpha_l U)}{U^3} dr \tag{A35}$$

which is similar to that of *Gelhar and Collins* [1971].

[57] **Acknowledgments.** This work was supported by the Assistant Secretary for Fossil Energy, Office of Oil Gas and Shale Technologies, of the U.S. Department of Energy under contract DE-AC03-76SF00098.

References

Anile, A. M., J. K. Hunter, P. Pantano, and G. Russo (1993), *Ray Methods for Nonlinear Waves in Fluids and Plasmas*, Longman Sci. and Tech., New York.

Arridge, S. (1999), Optical tomography in medical imaging, *Inverse Problems*, *15*, R41–R93.

Barenblatt, G. I. (1979), *Similarity, Self-Similarity, and Intermediate Asymptotics*, Consult. Bur., New York.

Bear, J. (1972), *Dynamics of Fluids in Porous Media*, Dover, Mineola, N. Y.

Bracewell, R. N. (1978), *The Fourier Transform and Its Applications*, McGraw-Hill, New York.

Carslaw, H. S., and J. C. Jaeger (1959), *Conduction of Heat in Solids*, Oxford Univ. Press, New York.

Chapman, S. J., J. M. H. Lawry, and J. R. Ockendon (1999), Ray theory for high-Peclet-number convection-diffusion, *SIAM J. Appl. Math.*, *60*, 121–135.

Cohen, J. K., and R. M. Lewis (1967), A ray method for the asymptotic solution of the diffusion equation, *J. Inst. Math. Appl.*, *3*, 266–290.

Courant, R., and D. Hilbert (1962), *Methods of Mathematical Physics*, Wiley-Interscience, New York.

Crane, M. J., and M. J. Blunt (1999), Streamline-based simulation of solute transport, *Water Resour. Res.*, *35*, 3061–3078.

Datta-Gupta, A., and M. J. King (1995), A semianalytical approach to tracer flow modeling in heterogeneous permeable media, *Adv. Water Resour.*, *18*, 9–24.

Datta-Gupta, A., L. W. Lake, and G. A. Pope (1995), Characterizing heterogeneous permeable media with spatial statistics and tracer data using sequential simulated annealing, *Math. Geol.*, *27*(6), 763–787.

Datta-Gupta, A., S. Yoon, D. W. Vasco, and G. A. Pope (2002), Inverse modeling of partitioning interwell tracer tests: A streamline approach, *Water Resour. Res.*, *38*(6), 1079, doi:10.1029/2001WR000597.

Davey, A., K. Karasaki, J. C. S. Long, M. Landsfeld, A. Mensch, and S. J. Martel (1989), Analysis of the hydraulic data from the MI Fracture Zone at the Grimsel Rock Laboratory, Switzerland, *LBNL Rep. 27864*, Lawrence Berkeley Natl. Lab., Berkeley.

de Marsily, G. (1986), *Quantitative Hydrogeology*, Academic, San Diego, Calif.

Dingle, R. B. (1973), *Asymptotic Expansions: Their Derivation and Interpretation*, Academic, San Diego, Calif.

Feyen, L., J. J. Gomez-Hernandez, P. J. Ribeiro, Jr., K. J. Beven, and F. De Smedt (2003), A Bayesian approach to stochastic capture zone delineation incorporating tracer arrival times, conductivity measurements, and hydraulic head observations, *Water Resour. Res.*, *39*(5), 1126, doi:10.1029/2002WR001544.

Fierz, T. (1993), Summary run 77, *Rep. 566*, Solexperts, Schwerzenbach, Switzerland.

Finsterle, S., and K. Pruess (1995), Solving the estimation-identification problem in two-phase flow modeling, *Water Resour. Res.*, *31*, 913–924.

Gardner, C. S., and G. K. Morikawa (1960), Similarity in the asymptotic behavior of collision-free hydromagnetic waves and water waves, *Rep. 90-9082*, Courant Inst. Math. Sci., New York.

Gelhar, L. W., and M. A. Collins (1971), General analysis of longitudinal dispersion in nonuniform flow, *Water Resour. Res.*, *7*, 1511–1521.

Georgescu, A. (1995), *Asymptotic Treatment of Differential Equations*, Chapman and Hall, New York.

Gordon, R., and G. T. Herman (1974), Three dimensional reconstruction from projections: A review of algorithms, *Int. Rev. Cytol.*, *38*, 111–151.

Grindrod, P. (1996), *The Theory and Applications of Reaction-Diffusion Equations*, Clarendon, Oxford, U. K.

Harvey, C. R., and S. M. Gorelick (1995), Mapping hydraulic conductivity: Sequential conditioning with measurements of solute arrival times, hydraulic head, and local conductivity, *Water Resour. Res.*, *31*, 1615–1626.

Iyer, H. M., and K. Hirahara (1993), *Seismic Tomography: Theory and Practice*, Chapman and Hall, New York.
Jeffrey, A., and T. Kawahara (1982), *Asymptotic Methods in Nonlinear Wave Theory*, Pitman, London.
Jeffrey, A., and T. Taniuti (1964), *Nonlinear Wave Propagation*, Academic, New York.
Karasaki, K., B. Freifeld, A. Cohen, K. Grossenbacher, P. Cook, and D. Vasco (2000), A multidisciplinary fractured rock characterization study at Raymond Field Site, Raymond, California, *J. Hydrol.*, *236*, 17–34.
King, M. J., and A. Datta-Gupta (1998), Streamline simulation: A current perspective, *In Situ*, *22*(1), 91–140.
Kline, M., and I. W. Kay (1979), *Electromagnetic Theory and Geometrical Optics*, Krieger, Huntington, N. Y.
Knessl, C., and J. B. Keller (1997), Advection-diffusion past a strip. II. Oblique incidence, *J. Math. Phys*, *38*, 267–282.
Knobloch, E., and J. De Luca (1990), Amplitude equations for traveling wave convection, *Nonlinearity*, *3*, 975–980.
Mauldon, A. D., K. Karasaki, S. J. Martel, J. C. S. Long, M. Landsfeld, A. Mensch, and S. Vomvoris (1993), An inversion technique for developing models for fluid flow in fracture systems using simulated annealing, *Water Resour. Res.*, *29*, 3775–3789.
Noble, B., and J. W. Daniel (1977), *Applied Linear Algebra*, Prentice-Hall, Old Tappan, N. J.
Noorishad, J., and C.-F. Tsang (1996), ROCMAS simulator: A thermohydromechanical computer code, in *Coupled Thermo-hydro-mechanical Processes of Fractured Media*, edited by J. Stephansson and C.-F. Tsang, pp. 551–558, Elsevier Sci., New York.
O'Sullivan, M. J., K. Pruess, and M. J. Lippmann (2001), State of the art of geothermal reservoir simulation, *Geothermics*, *30*, 395–429.
Paige, C. C., and M. A. Saunders (1982), LSQR: An algorithm for sparse linear equations and sparse linear systems, *Trans. Math. Software*, *8*, 195–209.
Parker, R. L. (1994), *Geophysical Inverse Theory*, Princeton Univ. Press, Princeton, N. J.
Press, W. H., S. A. Teukolsky, W. T. Vetterling, and B. P. Flannery (1992), *Numerical Recipes*, Cambridge Univ. Press, New York.
Pruess, K., C. Oldenburg, and G. Moridis (1999), TOUGH2 User's Guide, version 2.0, *LBNL Rep. 43134*, Lawrence Berkeley Natl. Lab., Berkeley, Calif.
Rittmann, B. E., and J. M. VanBriesen (1996), Microbiological processes in reactive modeling, in *Reactive Transport in Porous Media*, edited by P. C. Lichtner, C. I. Steefel, and E. H. Oelkers, *Rev. Mineral.*, *34*, 311–334.
Rubin, Y., and G. Dagan (1992), Conditional estimation of solute travel times in heterogeneous formations: Impact of the conductivity measurements, *Water Resour. Res.*, *28*, 1033–1040.
Rutqvist, J., Y.-S. Wu, C.-F. Tsang, and G. Bodvarsson (2002), A modeling approach for analysis of coupled multiphase fluid flow, heat transfer, and deformation in fractured porous rock, *Int. J. Rock Mech. Min. Sci.*, *39*, 429–442.
Sethian, J. A. (1999), *Level Set and Fast Marching Methods*, Cambridge Univ. Press, New York.
Smith, R. (1981), The early stages of contaminant dispersion in shear flows, *J. Fluid Mech.*, *111*, 107–122.
Solexperts (1989), Nagra migration long term constant Q test in BOMI 87.009, test analysis and description, *Rep. 566*, Zurich, Switzerland.
Tarantola, A. (1987), *Inverse Problem Theory*, Elsevier Sci., New York.
Vasco, D. W., and A. Datta-Gupta (1999), Asymptotic solutions for solute transport: A formalism for tracer tomography, *Water Resour. Res.*, *35*, 1–16.
Vasco, D. W., and A. Datta-Gupta (2001), Asymptotics, saturation fronts, and high resolution reservoir characterization, *Transp. Porous Media*, *42*, 315–350.
Vasco, D. W., and K. Karasaki (2001), Inversion of pressure observations: An integral formulation, *J. Hydrol.*, *253*, 27–40.
Vasco, D. W., A. Datta-Gupta, and J. C. S. Long (1997), Resolution and uncertainty in hydrologic characterization, *Water Resour. Res.*, *33*, 379–397.
Vasco, D. W., H. Keers, and K. Karasaki (2000), Estimation of reservoir properties using transient pressure data: An asymptotic approach, *Water Resour. Res.*, *36*, 3447–3465.
Virieux, J., C. Flores-Luna, and D. Gibert (1994), Asymptotic theory for diffusive electromagnetic imaging, *Geophys. J. Int.*, *119*, 857–868.
Wallach, R., and J.-Y. Parlange (2000), Applying the boundary layer concept to model transport of dissolved chemicals in preferential flow paths, *Water Resour. Res.*, *36*, 2845–2851.
Whitham, G. B. (1974), *Linear and Nonlinear Waves*, John Wiley, New York.
Woodbury, A. D., and Y. Rubin (2000), A full-Bayesian approach to parameter inference from tracer travel time moments and investigation of scale effects at the Cape Cod experiment site, *Water Resour. Res.*, *36*, 159–171.
Xu, T., and K. Pruess (2001), Modeling multiphase non-isothermal fluid flow and reactive geochemical transport in variably saturated fractured rocks: 1. Methodology, *Am. J. Sci.*, *301*, 16–33.
Xu, T., E. Sonnenthal, N. Spycher, K. Pruess, G. Brimhall, and J. Apps (2001), Modeling multiphase non-isothermal fluid flow and reactive geochemical transport in variably saturated fractured rocks: 1. Applications to supergene copper enrichment and hydrothermal flows, *Am. J. Sci.*, *301*, 34–59.
Yeh, G. T., and V. S. Tripathi (1991), A model for simulating transport of reactive multispecies components: Model development and demonstration, *Water Resour. Res.*, *27*, 3075–3094.
Yeh, W. W.-G. (1986), Review of parameter identification procedures in groundwater hydrology: The inverse problem, *Water Resour. Res.*, *22*, 95–108.

S. Finsterle and D. W. Vasco, Earth Sciences Division, Building 90, Berkeley Laboratory, 1 Cyclotron Road, Berkeley, CA 94720, USA. (dwvasco@lbl.gov)